Journal of
Synchrotron Radiation

ISSN 0909-0495

Received 4 February 2008
Accepted 30 June 2008

Polarization analysis in soft X-ray diffraction to study magnetic and orbital ordering

U. Staub,[a]* V. Scagnoli,[a,b] Y. Bodenthin,[a] M. García-Fernández,[a] R. Wetter,[a] A. M. Mulders,[a,c,d] H. Grimmer[e] and M. Horisberger[e]

[a]Swiss Light Source, Paul Scherrer Institut, 5232 Villigen PSI, Switzerland, [b]European Synchrotron Radiation Facility, BP 220, 38043 Grenoble Cedex, France, [c]Department. of Applied Physics, Curtin University of Technology, GPO Box U1987, Perth, WA 6845, Australia, [d]The Bragg Institute, Australian Nuclear Science and Technology Organization, Lucas Heights, NSW 2234, Australia, and [e]Laboratory for Developments and Methods, Paul Scherrer Institut, 5232 Villigen PSI, Switzerland. E-mail: urs.staub@psi.ch

An experimental approach to the analysis of charge, magnetic and orbital ordering in 3*d* transition-metal oxides is presented. The technique combines two important components: azimuthal rotations around the Bragg wavevector and polarization analysis of the Bragg intensities in the range 500–900 eV. The polarization analysis is performed using graded multilayers, which are translated and rotated in the vacuum chamber. It is shown why these two components are important to determine the origin of the Bragg scattered signals and how they allow us to separate the different contributions. Examples are given for the oxygen *K* and the Mn, Co, Ni and Cu $L_{2,3}$-edges, and the advantages and drawbacks of this experimental technique are discussed.

Keywords: resonant diffraction; charge, magnetic and orbital order.

1. Introduction

Resonant soft X-ray Bragg diffraction has developed in recent years into an important and very powerful technique for investigations of charge, magnetic and orbital ordering phenomena in solids. Initially, resonant soft X-ray scattering was mainly used to study magnetic problems (Tonnerre *et al.*, 1995) using reflectivity; nowadays, the technique is applied to magnetic domains (Dürr *et al.*, 1999) and more lately to bulk properties using Bragg diffraction. The first of these studies addressed magnetic and orbital ordering in manganites (Wilkins *et al.*, 2003; Dhesi *et al.*, 2004; Thomas *et al.*, 2004; Wilkins *et al.*, 2005), but the technique was soon applied to many other materials such as cuprates (Abbamonte *et al.*, 2004), nickelates (Schüssler-Langeheine *et al.*, 2005; Scagnoli *et al.*, 2006*a*,*b*), magnetite (Huang *et al.*, 2006), 4*f* electron materials (Mulders *et al.*, 2006, 2007; Ott *et al.*, 2006) and more recently also to multiferroics (Okamoto *et al.*, 2007; Bodenthin *et al.*, 2008). Most of these studies were concerned with the measurement of a Bragg reflection and its energy, temperature and, in the case of incommensurate structures, momentum dependence. In some cases X-rays with two different linear incoming polarizations were used. Very few studies used the freedom to rotate the sample around the scattering wavevector (azimuthal scan) to explore the behavior of the internal moments and their symmetry properties (Staub *et al.*, 2005; Wilkins *et al.*, 2005; Herrero-Marín *et al.*, 2006; Scagnoli *et al.*, 2006*a*), as is now standard for resonant hard X-ray Bragg diffraction (Paolasini *et al.*, 2007). Studies using polarization analysis of scattered radiation are even more rare (Staub *et al.*, 2005; Scagnoli *et al.*, 2006*a*). Note that polarization analysis was also recently applied to non-diffractive soft X-ray scattering (Braicovich *et al.*, 2007). As has been shown in the hard X-ray case, it is often crucial to perform polarization analysis and determine azimuthal angle dependence to be able to disentangle the contributions of charge, magnetic and orbital scattering and, in some cases, other more exotic tensorial contributions to the Bragg intensity (Lovesey *et al.*, 2007).

For resonant soft X-ray diffraction, such experiments are even more difficult since they require polarization analysis based on multilayers such as those used for the measurement of Faraday rotation (Kortright & Rice, 1995). Though polarization analysis using single-crystal Bragg reflections is not *a priori* impossible, the search for appropriate crystals and the need of high-precision adjustments for the analyzer make it a challenge. Similar problems exist for the use of single crystals as monochromators in the soft X-ray regime. Therefore, polarization analysis is based on multilayers and is used to characterize the polarization properties of beamlines producing variable polarization with, for example, Apple II undulators (Wang *et al.*, 2007). This type of insertion device can produce various polarizations (Sasaki *et al.*, 1993), *i.e.* circular plus and minus, linear with given variable axis, which are useful for the study of magnetic and orbital ordering phenomena. Also the azimuthal angle scans are non-trivial for soft X-ray diffractometers. The sample has to be in ultra-high

vacuum (UHV), particularly as the studied effects often occur at low temperatures. The motion around the Bragg wavevector needs both a re-adjustment of the tilt and incident angle for every azimuthal position, as the sample rotation axis is not necessary parallel to the Bragg wavevector (miscut angle). Correspondingly, only a tiny fraction of the published soft X-ray diffraction experiments use information obtained from the azimuthal angle dependence.

In this paper we present our set-up for azimuthal angle dependence in combination with polarization analysis using multilayers. We are able to collect all four linear polarization channels with this set-up. Moreover, we have the possibility to rotate the angle of the incident linear polarization and we can independently change the projection of the linear polarization direction of scattered X-rays within one quadrant of a circle in arbitrary steps. These two options allow a full Stokes parameter analysis of the scattered radiation. Examples of polarization analysis are given for the oxygen *K*-edge and Mn, Co, Ni and Cu $L_{2,3}$-edges, and we discuss how these results help clarify the origin of the scattering process.

2. Apparatus

For the soft X-ray diffraction experiments an improved version of the RESOXS end-station (Jaouen *et al.*, 2004) is used, which is connected to the SIM beamline at the Swiss Light Source of the Paul Scherrer Institut, Switzerland. The diffractometer uses a horizontal scattering geometry, and the two Apple II undulators of the beamline can produce variable linear (and circular) polarization, which is a powerful tool for X-ray magnetic linear and circular dichroism (Czekaj *et al.*, 2001). The polarization can be rotated a little more than a quarter turn (0 = horizontal to 90 = vertical), and not to negative angles. There are two different experimental set-ups today, one with an electromagnet ($H_{max} \simeq \pm 0.2$ T) and a limited tilt angle of $\pm 2^\circ$ (Jaouen *et al.*, 2004) and one without magnet and a maximum sample tilt angle of $\pm 10^\circ$, which is important for the measurements as a function of the azimuthal angle. The change of the azimuthal angle is performed manually by using the sample transfer system with which the sample can be exchanged and rotated on the cold finger of the cryostat. For that purpose the sample holder is equipped with three metal pins at 120° spacing to connect and/or rotate the sample. An angular scale on the sample transfer tube allows any azimuthal angle to be obtained within a precision of approximately 2°. This accuracy is sufficient for most studies of orbital and magnetic orderings.

The analyzer system is mounted on a large ring, which acts as a 2θ arm. The 2θ arm is able to perform a full 360° rotation. On the same arm, other detectors such as a photodiode and a water-cooled in-vacuum CCD camera can be simultaneously mounted, as can be see from Fig. 1. The diode is used to align the Bragg reflection and the detector can be switched by rotating the 2θ arm by the angle between the two detector set-ups. The in-vacuum CCD camera is very sensitive and allows us to measure weak signals with reduced noise levels. It has recently been used for the first resonant soft X-ray powder diffraction experiments (Staub *et al.*, 2007; García-Fernández *et al.*, 2008*a*). The polarization analyzer is shown in Fig. 2(*a*). Its main component is a graded W/C multilayer mounted at the Brewster angle (45°), which inherently suppresses the

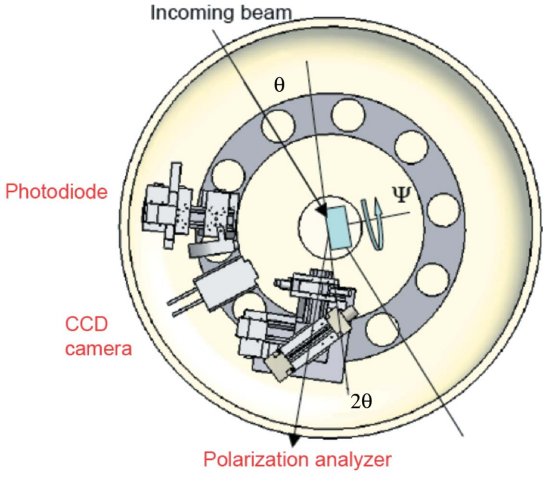

Figure 1
Sketch of the RESOXS scattering station at the SIM beamline of the Swiss Light Source, showing the large 2θ arm (ring with circles) and the mounting of the different detectors.

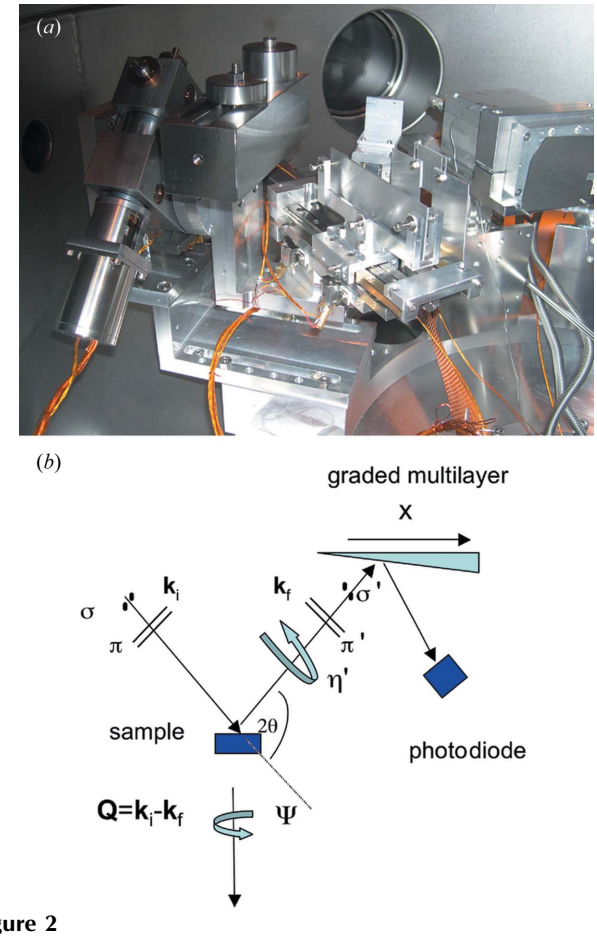

Figure 2
(*a*) Photograph of the analyzer station mounted in the open RESOXS chamber. (*b*) Schematic of the polarization analyzer for resonant soft X-ray scattering in the RESOXS chamber.

scattering of the X-rays with polarization lying in the scattering plane of the analyzer. A sketch of the scattering geometry is shown in Fig. 2(*b*). The polarization channels are defined as σ polarization for X-ray polarization lying perpendicular to the scattering plane and π polarization for polarization lying in the scattering plane. The important degrees of freedom are represented here by the azimuthal angle Ψ of the sample, the rotation η (a rotation of the analyzer stage around the scattered light direction $\mathbf{k}_f$), and the translation x of the graded multilayer with constant incidence angle.

The rotation η' and translation x of the analyzer are performed with *in situ* UHV motors. The motion ranges from approximately $+10^\circ$ to -100°. The angular range is limited by the available space (hitting the top flange with the analyzer) and the torque of the in-vacuum motors. Here 0 is defined as the vertical position of the analyzer, corresponding to a polarization of π in the scattered radiation from the sample. Note that the definition of the handedness of the two rotations is the same, indicating that a measurement of the same incident and exit angles of polarizations is not possible in this set-up, except for angles close to 0° and 90°.

The graded multilayers have been made by magnetron sputtering at PSI and have been proposed and used for polarization analysis earlier (Kortright & Rice, 1995; Mertins *et al.*, 1998). A Cu $K\alpha$ reflectivity scan is shown in Fig. 3(*a*). The multilayers are made of 100 bilayers of equally thick W and C layers, with the bilayer thickness adjusted to the wavelength requirement of the experiment. A soft X-ray reflectivity spectrum of one multilayer is shown in Fig. 3(*b*). The interference dip around 16° is a clear indication of an oxidized top layer, which also affects the reflectivity at the multilayer Bragg peak. However, owing to the large number of bilayers, the performance of the multilayer is reasonable. The main limitation in performance is due to interdiffusion and roughness at the interfaces of the multilayer. This problem could likely be reduced by using UHV growth conditions. This effect plays a dramatic role for very thin multilayers required for energies above 900 eV, as will be discussed later.

The relative polarization leakage (*i.e.* the ratio of the undesired suppressed polarization to the desired polarization) is typically very small, of the order of 0.1%, and does not significantly depend on the energy, as exemplified in Fig. 4(*a*). The reflectivity, however, decreases continuously for increasing energies and is of the order of a few percent at 650 eV, and more than two orders of magnitude weaker at 950 eV. The energy-dependent reflectivity of the multilayer used for the Ni edge is shown in Fig. 5(*a*). Above 950 eV the reflected signal is of the order of the fluorescence light emitted from the multilayer, and this set-up therefore is not useful for higher energies. The gradient of the multilayer is chosen in such a way that the energy broadening it causes at a given aperture and multilayer position does not significantly affect the peak reflectivity of the multilayer (see Fig. 4*b*). Consequently the length of the multilayer and its translation of approximately 90 mm cover one pair of transition-metal ion $L_{2,3}$-edges. This implies that for every experiment performed

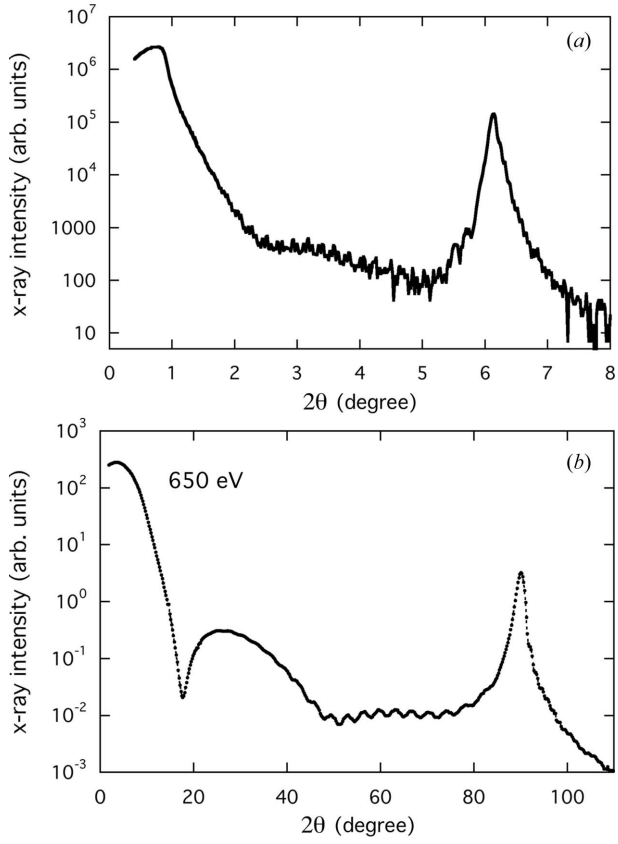

Figure 3
(*a*) Reflectivity of a W/C multilayer taken with Cu $K\alpha$ radiation. (*b*) Reflectivity curve of the multilayer in the direct beam using the optimal position x for 650 eV, in the vicinity of the Mn L-edges with σ incident radiation with respect to the scattering plane of the multilayer.

at a different absorption edge a different multilayer must be mounted and aligned. Such a multilayer change requires breaking the vacuum and often necessitates a new bake-out. We note that, for most samples studied so far, a larger multilayer gradient combined with a smaller aperture will not necessarily improve the efficiency, as even a well focused beam on the sample will lead to a broad spot of the Bragg peak at the multilayer position owing to the strong absorption at the absorption edge. Fig. 5(*b*) shows the position of the reflection maximum as a function of energy for several translations x of the multilayer. The variation in energy is caused by the gradient of the d spacing.

3. Application to charge, magnetic and orbital scattering

3.1. General considerations

We are interested here in the dipole ($E1$–$E1$) transitions $1s$–$2p$ for oxygen, $2p$–$3d$ for transition-metal ions and $3d$–$4f$ for rare-earth ions, because these transitions lie in the soft X-ray regime. $E2$ (quadrupole) transitions are typically not observed, as they resonate to electronic shells which are broad and empty with correspondingly weak diffraction.

Charge, magnetic and orbital terms may contribute to the structure factor of the Bragg reflection. Particularly inter-

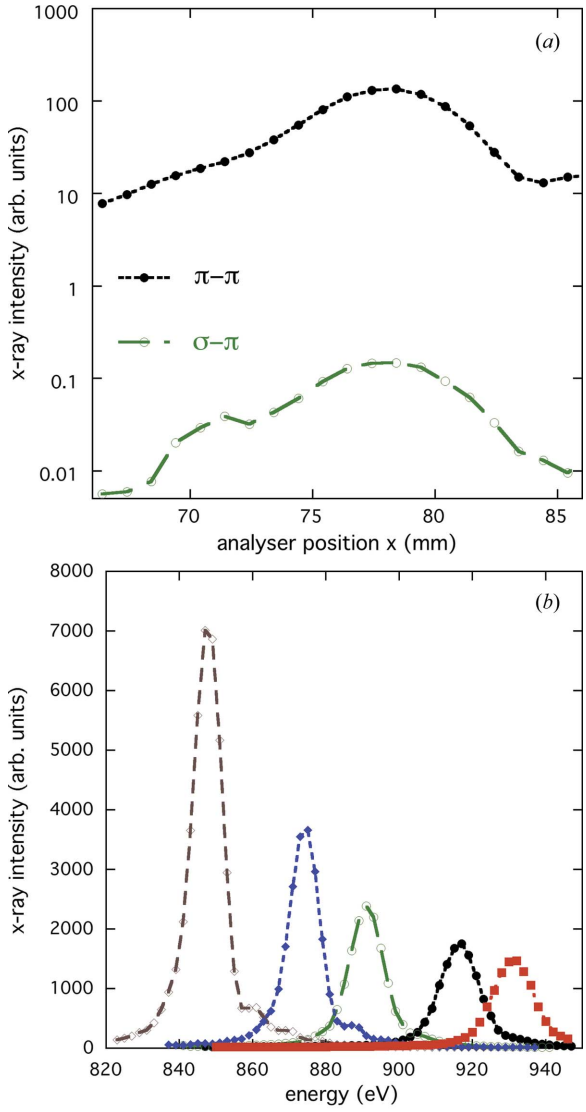

Figure 4
(*a*) Leakage of the multilayer as a function of multilayer translation demonstrated for an energy at the Ni L_3-edge (861 eV). (*b*) Reflected X-ray intensity as a function of energy. Each curve corresponds to a different x translation that satisfies the Bragg diffraction condition of the multilayer.

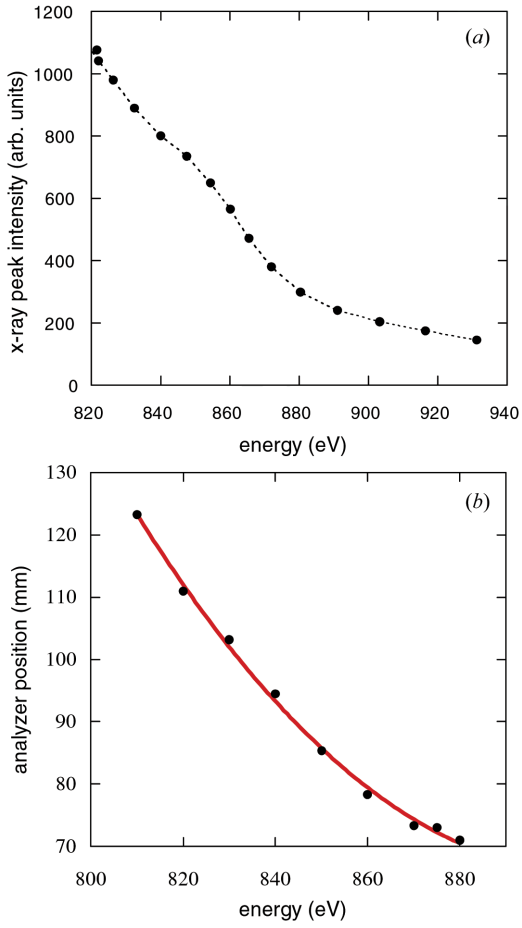

Figure 5
(*a*) Maximum reflected intensity from the multilayer as a function of incident energy. (*b*) Translation of the multilayer (analyzer position) to achieve this maximum. The solid curve shows a quadratic fit used for calibration.

esting is the case of charge order, as it involves a charge allowed reflection, often with an orbital contribution called the anisotropic tensor of susceptibility.

The X-ray scattering factor can be written as

$$f(E) = f_c(Q, E) + f_{mag}(E) + f_{orb}(E), \qquad (1)$$

where the charge term contains the Q-dependent Thomson term. All resonant terms $f(E)$ are described by a real and imaginary part, which are correlated with each other by the Kramers–Kronig transformation. The first term can be represented by a tensor of rank 0, a spherical object which is simply charged, and hence will not yield an azimuthal angle dependence. The magnetic and orbital terms are represented by tensors of rank 1 and 2, respectively, and a rotation of the azimuthal angle changes the scattered intensity. For the polarization dependence of the different terms, we refer to the review by Lovesey *et al.* (2005), where the polarization dependence of the structure factor is represented by a tensor X_Q^K in a given axis setting. Here K is the rank of the tensor and Q is its projection. For charge scattering, the relevant tensor X_0^0 is zero for the σ–π' and π–σ' channels, and the σ–σ' and π–π' channels differ by a factor $\cos(2\theta)$. For magnetic scattering, the σ–σ' channel is absent while the π–π' channel is proportional to $\sin(2\theta)$ and characterized by X_0^1. This tensor describes the magnetic moment along the z axis, in the crystal axis reference frame. The channels of the rotated light, σ–π' and π–σ', are characterized by X_1^1 and have an opposite complex phase which depends on the scattering angle as well as opposite sign. This can lead to a phase shift of π in their azimuthal angle dependence. The situation for orbital scattering, characterized by tensors X_Q^2, is more complex, and all four polarization channels may be allowed and may depend on the azimuth. In general, the intensities of the π–π' and σ–σ' channels are not equal, unless only the X_1^2 terms contribute. The rotated channels exhibit opposite complex phases but without the sign change exhibited by the magnetic contribution. These distinct Ψ-dependences allow us to extract the origin of the resonant diffraction. Note that some conclusions

can already be drawn when the incident polarization is switched between σ and π, without polarization analysis of the scattered radiation.

3.2. Examples

3.2.1. Oxygen *K*-edge. Ordering phenomena studied at the oxygen *K*-edge have been presented on cuprates (Abbamonte *et al.*, 2004) on the one hand and magnetite (Huang *et al.*, 2006) and manganites (Grenier *et al.*, 2007) on the other. Whereas in the first case, based on spectroscopic arguments, the observed Bragg reflection was interpreted as being due to a charge order at the oxygen site, for the second case the origin could not be directly specified; it was interpreted in the general scheme of orbital and charge ordering. The cuprate experiment was performed with only a single incident polarization, which does not allow any further conclusions on the origin of the reflection. The magnetite experiment was performed with σ and π incident radiation and found $I_\pi > I_\sigma$. The (0 0 1/2) reflection in magnetite is therefore not caused solely by charge order at the oxygen, although a contribution could exist. In the case of $Bi_{1-x}Ca_xMnO_3$, the Bragg reflection (0 0.31 0) occurring at the oxygen *K*-edge (Grenier *et al.*, 2007) has equal intensity for the incident π and σ channels (again taken without polarization analysis). From the dependence of the different tensors on the polarization, the authors conclude that the signal is in the rotated light channel only. Therefore, this (0 0.31 0) Bragg reflection represents the orbital ordering of the oxygen 2*p* states, likely induced by the combined orbital and charge ordering of the Mn ions.

The situation in $La_{7/8}Sr_{1/8}MnO_3$ is more complex. There are two features in the oxygen *K*-edge spectra of the (0 0 1/2) reflection with a different incident polarization dependence (Grenier *et al.*, 2007). The significant observed non-resonant charge scattering combined with the azimuthal angle dependence of the signal can be interpreted in terms of charge ordering occurring at the oxygen site (Grenier *et al.*, 2007). Here we show the same features in the spectra using polarization analysis for σ-scattered radiation and different incident polarizations in Fig. 6. The strong signal in the σ–σ channel and the weaker signal in the rotated channel indicate that an orbital signal is superimposed on that of the charge order. The complex behavior of the diffraction signals found at the oxygen *K*-edge gives clear indication that azimuthal scans and polarization analysis are indispensable tools for an unambiguous and more detailed interpretation, which is in progress.

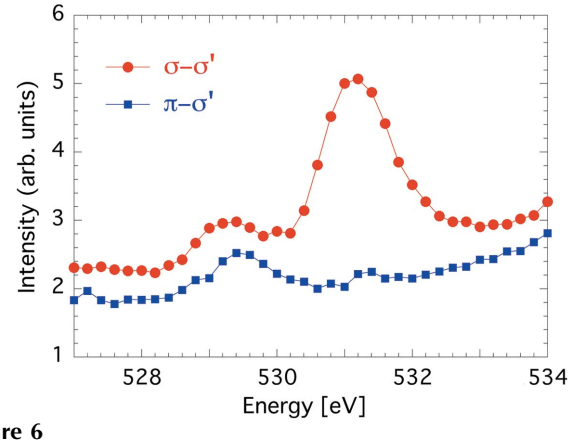

Figure 6
Energy dependence of the (0 0 1/2) reflection taken at the O *K*-edge at 30 K of $La_{7/8}Sr_{1/8}MnO_3$ for two different incident polarizations.

3.2.2. Mn $L_{2,3}$-edges. Polarization analysis has been used in the study of the orbital (1/4 1/4 0) reflection of $La_{0.5}Sr_{1.5}MnO_4$ at the Mn $L_{2,3}$-edges (Staub *et al.*, 2005). Fig. 7 shows the energy scans in all four polarization channels. The azimuthal angle dependence and the polarization analysis were used to demonstrate the presence of an additional magnetic signal contributing to the orbital reflection below T_N. The absence of a signal in the unrotated light channels is particular for this type of orbital ordering. Theoretical calculations have shown (Stojic *et al.*, 2005) that the polarization dependence can also be used to test possible magnetic structures. Some magnetic models break the symmetry at the Mn sites and lead to scattering in the unrotated light channels (σ–σ' and π–π'), which is not observed, as shown in Fig. 7.

3.2.3. Co $L_{2,3}$-edges. We study $GdBaCo_2O_{5.5-x}$, a layered cobaltite with complex and interesting electronic and magnetic properties (Maignan *et al.*, 1999). The energy and polarization dependence of the magnetic (0 0 1/2) reflection are shown in Figs. 8(*a*) and 8(*b*)–8(*c*), respectively. Owing to the layered structure the sample is plate-like. This makes the contribution from total reflectivity to the scattering significant even at large diffraction angle. The resonant diffracted intensity can be separated from the total reflectivity by performing *q* scans and recording integrated intensities. Even though this gives the most precise energy dependence, these scans are not often performed because they consume

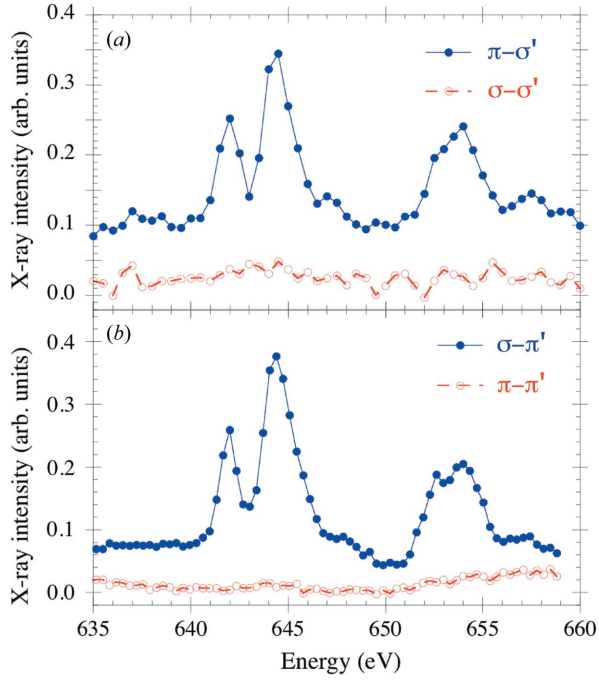

Figure 7
Energy scans of the (1/4 1/4 0) reflection of $La_{0.5}Sr_{1.5}MnO_4$ with polarization analysis of the scattered radiation, taken in the antiferromagnetic phase.

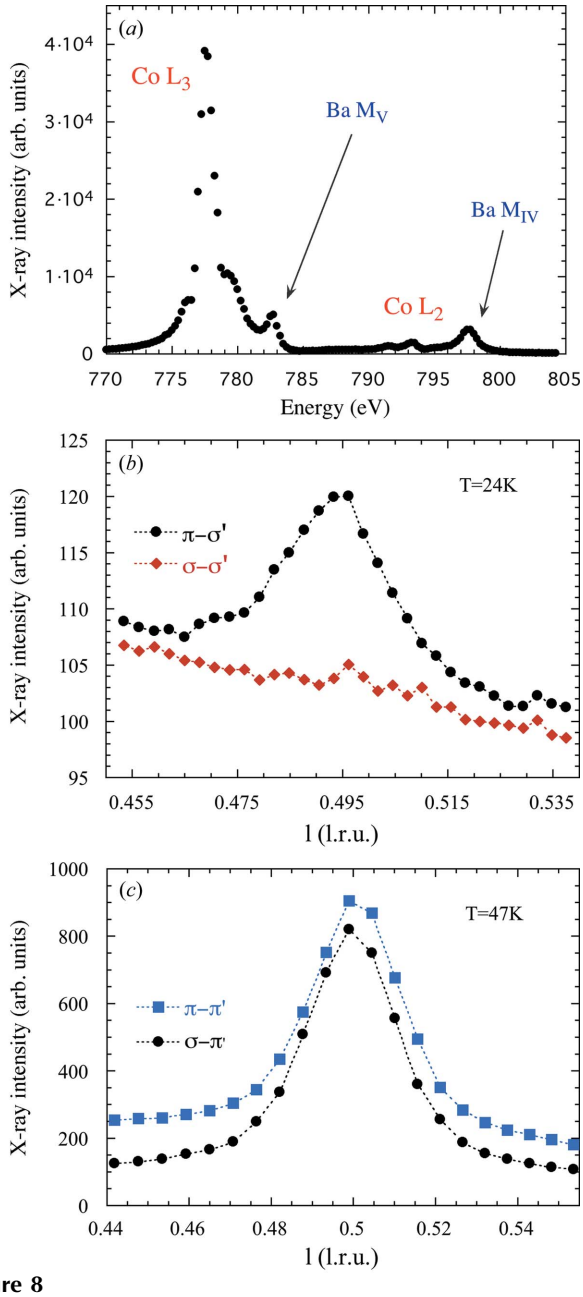

Figure 8
(*a*) Energy dependence of the (0 0 1/2) reflection taken with π incident radiation (without polarization analysis) in the antiferromagnetic phase. (*b*, *c*) All four polarization channels of the resonant (0 0 1/2) reflection taken at the Co L_3-edge at 777.5 eV.

approximately 20 times more beam time. Another possibility is to use polarization analysis and record the rotated light channel, as this will suppress the anomalous charge reflectivity. This will be published elsewhere (García-Fernández *et al.*, 2008*b*). Performing a polarization analysis shows here that the scattering at the Co L_3-edge is of magnetic origin. The Bragg peak is absent in the σ–σ channel, but appears in the other three, giving direct proof that the Bragg peak is of magnetic origin, as shown in Figs. 8(*b*) and 8(*c*).

3.2.4. Ni $L_{2,3}$-edges. Polarization analysis in combination with azimuthal angle scans were performed for the Ni $L_{2,3}$-edges in $NdNiO_3$ (Scagnoli *et al.*, 2006*a*,*b*). The polarization analysis clearly demonstrated the magnetic origin of the (1/2 0 1/2) reflection, without a detectable orbital contribution. The sample was a thin epitaxial film and the scattering intensity was broad and rather weak. Moreover, the reflectivity of the multilayer is significantly reduced at this incident energy range, which makes the polarization analysis challenging. This limited the polarization analysis to the maximum intensity at the Ni L_3-edge signal. Additional information could in principle be extracted by performing a polarization analysis at every azimuth. Although this is possible, it is often hampered by the weak signals, which require longer counting times and possibly several scans. The azimuthal angle dependence contains systematic errors, which are difficult to correct for. The intensities cannot be calibrated with a strong lattice reflection as typically done in the hard X-ray regime, because these lie in most cases outside the Ewald sphere in the soft X-ray regime. The most accurate method is to consider the ratio of σ to π, with or without the analysis of the polarization of the scattered radiation. In the case of $NdNiO_3$, the azimuthal angle scan allowed us to distinguish between different magnetic structures (Scagnoli *et al.*, 2006*a*), which were indistinguishable in neutron powder diffraction.

3.2.5. Cu $L_{2,3}$-edges. Energy scans with σ and π incident polarization of the (0 0 1) Bragg reflection of the high-T_c superconductor $YBa_2Cu_3O_7$ are shown in Fig. 9. Symmetry analysis shows that there is charge scattering (Thomson and resonant) and, in addition, one orbital tensor is allowed; however, the relative weights are unknown. The diffracted intensities are

$$I^{\pi} = \left|F_c \cos(2\theta) + F_{orb}^{\pi-\pi'}\right|^2 + \left|F_{orb}^{\pi-\sigma'}\right|^2,$$
$$I^{\sigma} = \left|F_c + F_{orb}^{\sigma-\sigma'}\right|^2 + \left|F_{orb}^{\sigma-\pi'}\right|^2.$$

Here c denotes the charge and orb the orbital (or quadrupole) contributions. The clear difference in spectra recorded with σ and π incident radiation points to a strong interference between charge and orbital diffraction. Energy scans recorded

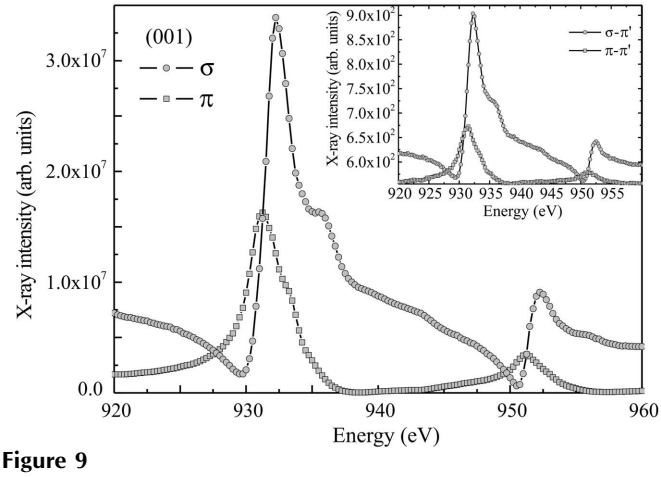

Figure 9
Energy dependence of the charge-allowed (0 0 1) reflection of $YBa_2Cu_3O_7$ taken at ambient temperatures with π and σ incident radiation without polarization analysis. This inset shows the σ–π' and π–π' channels. The lines are guide for the eyes.

with polarization analysis are shown for σ–π' and π–π' in the inset of Fig. 9. In this experiment there are several complications. The intensity collected with the analyzer contains no significant fluorescence contribution originating from the sample but is dominated by the fluorescence arising from the multilayer. The intensity is therefore proportional to the scattered signal of the Bragg reflection without polarization analysis. Further, one has to take into account the absorption of the scattered signal at the Cu edge, which is very anisotropic. Note in this case that this anisotropy is directly related to the strong orbital contribution in the scattered signal. Hence, these complications, in part caused by the decreased efficiency of the multilayer at these energies, show the limitations of the existing set-up. Work on the disentanglement of the different contributions is in progress; however, at this stage it is not certain if the data quality is sufficient for quantitative results.

4. Full polarization analysis of the scattered radiation

We have upgraded the experimental set-up to allow a full polarimetry analysis in soft X-ray scattering experiments yielding access to all three Poincaré–Stokes parameters. In complex systems a non-trivial intensity pattern in conventional energy scans across the resonance edges could often be observed. This may be the result of multiple scattering processes. The interference of multiple scattering processes can lead to phase shifts between the respective scattering amplitudes, giving rise, for instance, to a conversion of linearly polarized light into circularly polarized light. A complete polarization analysis will allow these multiple scattering processes, *e.g.* when several atomic multipoles are involved in the scattering event, to be disentangled as was nicely demonstrated recently for resonant hard X-ray diffraction (Mazzoli *et al.*, 2007). A full polarization analysis means full access to all possible linear polarizations between σ and π of the scattered and incident beam.

Experimentally, we rotate the linearly polarized incident light by an angle η between σ and π polarization and measure the scattered intensity at the angle η'. The Poincaré–Stokes parameters,

$$P_1 = \left(\left|E_1'\right|_2 - \left|E_2'\right|_2\right)/P_0,$$
$$P_2 = 2\,\mathrm{Re}(E_1'^{*}E_2')/P_0,$$
$$P_3 = 2\,\mathrm{Im}(E_1'^{*}E_2')/P_0,$$

can be obtained by fitting the measured intensity to (Spencer & Wolf, 1953)

$$I(\eta, \eta') = I_2/2\left[1 + P_1(\eta)\cos 2\eta' + P_2(\eta)\sin 2\eta'\right].$$

Here, $P_0 = (|E_1'|^2 + |E_2'|^2)$ is the total intensity, and $E_1'^{*}$ is the complex conjugate of E_1'. P_1 and P_2 describe the linear polarization states, while P_3 indicates the degree of circular polarization. Fig. 10 shows $I(\eta, \eta')$ measured at the (1/2 0 1/4) reflection of $ErMn_2O_5$, measured at T = 37 K. The (1/2 0 1/4) reflection in $ErMn_2O_5$ is predominantly of magnetic origin and is caused by the non-collinear magnetic structure. At the measured temperature the system is in the commensurate magnetic state (Bodenthin *et al.*, 2008). A non-trivial intensity pattern is observed with maximum intensity in the rotated light channels (π–σ', σ–π'), which is assigned to scattering multipoles of different ranks. Such a non-trivial intensity pattern may arise by admixture of induced charge (aspherical charge density) contribution and magnetic scattering. Unfortunately, owing to technical reasons, the background could not be determined yet. A detailed analysis at different temperatures as well as an improved background correction will be carried out in future studies.

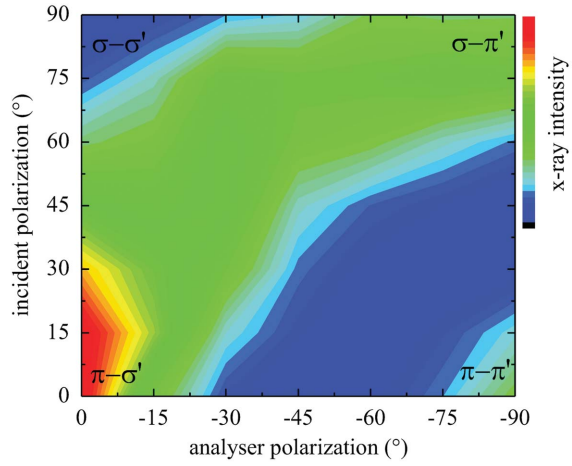

Figure 10
Full polarimetry pattern of the (1/2 0 1/4) reflection of $ErMn_2O_5$ measured at T = 37 K. The maximum intensity in the rotated light channel (π–σ', σ–π') is caused by the magnetic contribution to the scattering peak.

5. Outlook and conclusions

We have presented a set-up for soft X-ray resonant diffraction including azimuthal rotation and polarization analysis of the diffracted radiation. The analyzer system utilizes graded multilayers. Energy-dependent polarization analysis is performed by translation of the graded multilayer, which adjusts the d-spacing of the Bragg reflection to the required energy. It is shown that polarization analysis and azimuthal rotations are indispensable for understanding the origin of the observed Bragg diffraction. Polarization analysis is feasible in the softer X-ray regime but approaches its limit at the Cu $L_{2,3}$-edges. Full polarization analysis of the scattered radiation is possible, and may be helpful when different tensorial contributions interfere with each other. Extension of the energy range of a single multilayer would yield a system that does not require breaking the vacuum when changing the absorption edge. Further improvements of detector technology and multilayer growth would strongly improve the performance of the polarization analyzer system and may extend its energy range to cover the rare-earth $M_{4,5}$-edges. Finally, a scheme for efficiency correction will be developed for rotation (η') around the outgoing beam.

We thank the beamline staff of X11MA for their excellent technical support, J.-M. Tonnerre for providing experimental

equipment, and S. Grenier for his support. This work was supported by the Swiss National Science Foundation. Experiments were performed at SLS of the Paul Scherrer Institut, Villigen PSI, Switzerland.

References

Abbamonte, P., Blumberg, G., Rusydi, A., Gozar, A., Evans, P. G., Siegrist, T., Venema, L., Eisaki, H., Isaacs, E. D. & Sawatzky, G. A. (2004). *Nature (London)*, **431**, 1078.

Bodenthin, Y., Staub, U., García-Fernández, M., Janoschek, M., Schlappa, J., Golovenchits, E. I., Sanina, V. A. & Lushnikov, S. G. (2008). *Phys. Rev. Lett.* **100**, 027201.

Braicovich, L., van der Laan, G., Tagliaferri, A., Annese, E., Ghiringhelli, G. & Brookes, N. B. (2007). *Phys. Rev. B*, **75**, 184408.

Czekaj, S., Nolting, F., Heydermann, L. J., Willmott, P. R. & van der Laan, G. (2001). *Phys. Rev. B*, **73**, 020401.

Dhesi, S. S., Mirone, A., De Nadai, C., Ohresser, P., Bencok, P., Brookes, N. B., Reutler, P., Revcolevschi, A., Tagliaferri, A., Toulemonde, O. & van der Laan, G. (2004). *Phys. Rev. Lett.* **92**, 056403.

Dürr, H., Dudzik, E., Dhesi, S., Goedkoop, J., van der Laan, G., Belakhovsky, M., Mocuta, C., Marty, A. & Samson, Y. (1999). *Science*, **284**, 2166–2168.

García-Fernández, M. *et al.* (2008*a*). In preparation.

García-Fernández, M., Staub, U., Bodenthin, Y., Lawrence, S. M., Mulders, A. M., Buckley, C. E., Weyeneth, S., Pomjakushina, E. & Conder, K. (2008*b*). *Phys. Rev. B*, **77**, 060402.

Grenier, S., Thomas, K. J., Hill, J. P., Staub, U., Bodenthin, Y., García-Fernández, M., Scagnoli, V., Kiryukhin, V., Cheong, S.-W., Kim, B. G. & Tonnerre, J. M. (2007). *Phys. Rev. Lett.* **99**, 206403.

Herrero-Marín, J., García, J., Subias, G., Blasco, J., Concepción-Sanchez, M. & Stanescu, S. (2006). *Phys. Rev. B*, **73**, 224407.

Huang, D. J., Lin, H.-J., Okamoto, J., Chao, K. S., Jeng, H.-T., Guo, G. Y. H., Hsu, C.-H., Huang, C.-M., Ling, D. C., Wu, W. B., Yang, C. S. & Chen, C. T. (2006). *Phys. Rev. Lett.* **96**, 96401.

Jaouen, N., Tonnerre, J.-M., Kapoujian, G., Taunier, P., Roux, J.-P., Raoux, D. & Sirotti, F. (2004). *J. Synchrotron Rad.* **11**, 353–357.

Kortright, J. B. & Rice, M. (1995). *Phys. Rev. B*, **51**, 10240–10243.

Lovesey, S. W., Balcar, E., Knight, K. S. & Fernandez-Rodriguez, J. (2005). *Phys. Rep.* **411**, 233–289.

Lovesey, S. W., Fernández-Rodríguez, J., Blanco, J. A., Sivia, D. S., Knight, K. S. & Paolasini, L. (2007). *Phys. Rev. B*, **75**, 014409.

Maignan, A., Martin, C., Pelloquin, D., Nguyen, N. & Raveau, B. (1999). *J. Solid State Chem.* **142**, 247–260.

Mazzoli, C., Wilkins, S. B., Di Matteo, S., Detlefs, C., Scagnoli, V., Paolasini, L. & Ghigna, P. (2007). *Phys. Rev. B*, **76**, 195118.

Mertins, H. C., Schäfers, F., Grimmer, H., Clemens, D., Böni, P. & Horisberger, M. (1998). *Appl. Opt.* **37**, 1873–1882.

Mulders, A. M., Staub, U., Scagnoli, V., Lovesey, S. W., Balcar, E., Nakamura, T., Kikkawa, A., van der Laan, G. & Tonnerre, J. M. (2006). *J. Phys. Condens. Matter*, **18**, 11195–11202.

Mulders, A. M., Staub, U., Scagnoli, V., Tanaka, Y., Kikkawa, A., Katsumata, K. & Tonnerre, J. M. (2007). *Phys. Rev. B*, **75**, 184438.

Okamoto, J., Huang, D. J., Mou, C.-Y., Chao, K. S., Lin, H.-J., Park, S., Cheong, S.-W. & Chen, C. T. (2007). *Phys. Rev. Lett.* **98**, 157202.

Ott, H., Schüssler-Langeheine, C., Schierle, E., Grigotiev, A. Y., Leiner, V., Zabel, H., Kaindl, G. & Weschke, E. (2006). *Phys. Rev. B*, **74**, 094412.

Paolasini, L. *et al.* (2007). *J. Synchrotron Rad.* **14**, 301–312.

Sasaki, S., Kakuno, K., Takada, T., Shimada, T., Yanagida, K. & Miyahara, Y. (1993). *Nucl. Instrum. Methods Phys. Res. A*, **331**, 763–767.

Scagnoli, V., Staub, U., Mulders, A. M., Janousch, M., Meijer, G. I., Hammerl, G., Tonnerre, J. M. & Stojic, N. (2006*a*). *Phys. Rev. B*, **73**, 100409(R).

Scagnoli, V., Staub, U., Mulders, A. M., Meijer, G. I., Hammerl, G. & Tonnerre, J. M. (2006*b*). *Physica B*, **378–380**, 541–542.

Schüssler-Langeheine, C. *et al.* (2005). *Phys. Rev. Lett.* **95**, 156402.

Spencer, L. V. & Wolf, C. (1953). *Phys. Rev.* **90**, 510–514.

Staub, U., García-Fernández, M., Mulders, A. M., Bodenthin, Y., Martínez-Lope, M. J. & Alonso, J. A. (2007). *J. Phys. Condens. Matter*, **19**, 092201.

Staub, U., Scagnoli, V., Mulders, A. M., Katsumata, K., Honda, Z., Grimmer, H., Horisberger, M. & Tonnerre, J. M. (2005). *Phys. Rev. B*, **71**, 214421.

Stojic, N., Binggeli, N. & Altarelli, M. (2005). *Phys. Rev. B*, **72**, 104108.

Thomas, K. J., Hill, J. P., Grenier, S., Kim, Y.-J., Abbamonte, P., Venema, L., Rusydi, A., Tomioka, Y., Tokura, Y., McMorrow, D. F. & van Veenendaal, M. (2004). *Phys. Rev. Lett.* **92**, 237204.

Tonnerre, J. M., Séve, L., Raoux, D., Soullié, G., Rodmacq, B. & Wolfers, P. (1995). *Phys. Rev. Lett.* **75**, 740–743.

Wang, Z. *et al.* (2007). *Appl. Phys. Lett.* **90**, 081910.

Wilkins, S. B., Hatton, P. D., Roper, M. D., Prabhakaran, D. & Boothroyd, A. T. (2003). *Phys. Rev. Lett.* **90**, 187201.

Wilkins, S. B., Stojic, N., Beale, T. A. W., Binggeli, N., Castleton, C. W. M., Bencok, P., Prabhakaran, D., Boothroyd, A. T., Hatton, P. D. & Altarelli, M. (2005). *Phys. Rev. B*, **71**, 245102.